Full length article

# A simple approach for the estimation of $CO_2$ penetration depth into a caprock layer

CrossMark

J.G. Wang [a,b,*], Yang Ju [b,c], Feng Gao [a,b], Jia Liu [b]

[a] School of Mechanics and Civil Engineering, China University of Mining and Technology, Xuzhou, 221116, China
[b] State Key Laboratory for Geomechanics and Deep Underground Engineering, China University of Mining and Technology, Xuzhou, 221116, China
[c] State Key Laboratory of Coal Resources and Safe Mining, China University of Mining and Technology, Beijing, 100083, China

## ARTICLE INFO

## ABSTRACT

Caprock is a water-saturated formation with a sufficient entry capillary pressure to prevent the upward migration of a buoyant fluid. When the entry capillary pressure of caprock is smaller than the pressure exerted by the buoyant $CO_2$ plume, $CO_2$ gradually penetrates into the caprock. The $CO_2$ penetration depth into a caprock layer can be used to measure the caprock sealing efficiency and becomes the key issue to the assessment of caprock sealing efficiency. On the other hand, our numerical simulations on a caprock layer have revealed that a square root law for time and pore pressure exists for the $CO_2$ penetration into the caprock layer. Based on this finding, this study proposes a simple approach to estimate the $CO_2$ penetration depth into a caprock layer. This simple approach is initially developed to consider the speed of $CO_2$ invading front. It explicitly expresses the penetration depth with pressuring time, pressure difference and pressure magnitude. This simple approach is then used to fit three sets of experimental data and good fittings are observed regardless of pressures, strengths of porous media, and pore fluids (water, hydrochloric acid, and carbonic acid). Finally, theoretical analyses are conducted to explore those factors affecting $CO_2$ penetration depth. The effects of capillary pressure, gas sorption induced swelling, and fluid property are then included in this simple approach. These results show that this simple approach can predict the penetration depth into a caprock layer with sufficient accuracy, even if complicated interactions in penetration process are not explicitly expressed in this simple formula.

© 2016 Institute of Rock and Soil Mechanics, Chinese Academy of Sciences. Production and hosting by Elsevier B.V. All rights reserved.

## 1. Introduction

Acidic fluids intrusion is a severe potential hazard for the geological storage of carbon dioxide ($CO_2$) in underground formations (Rutqvist and Tsang, 2002; Vilarrasa et al., 2014; Abidoye et al., 2015; Fei et al., 2015). The $CO_2$ leakage from a caprock layer may seriously reduce the quality of fresh water in the shallow subsurface and change the local air quality on the earth surface (Rutqvist et al., 2010; Armitage et al., 2013, 2015; Li et al., 2013). For example, the flow-through leakage of $CO_2$ may change the precipitation pattern when the penetration depth reaches the top of the caprock layer or the occurrence of breakthrough (Heath et al., 2012; Bolourinejad and Herher, 2014; Bielicki et al., 2015). This $CO_2$ breakthrough may heavily pollute the upper fresh water

aquifer (Tsang et al., 2008; Bricker et al., 2012; Fontenot et al., 2013; Yang et al., 2013) if the multilayer system of caprocks is penetrated (Birkholzer et al., 2009). The subsequent flow-through leakage may be of self-enhancement or self-limiting (sometimes called self-healing) due to geochemical interaction (Deng et al., 2013; Ellis et al., 2013; Huerta et al., 2013; Smith et al., 2013; Elkhoury et al., 2015). Therefore, the caprock sealing efficiency is the key safety issue to the containment of a $CO_2$ storage reservoir.

The assessment of $CO_2$ penetration depth into a caprock layer becomes one of main tasks for $CO_2$ storage potential evaluations (Huang et al., 2014; Wriedt et al., 2014; Deng et al., 2015; Song et al., 2015). The assessment can be implemented through site investigations and observations, laboratory tests, and numerical simulations. Numerical simulation is an essential tool in fully understanding the migration of injected $CO_2$ for commercial-scale sequestration projects (Doughty, 2010; Rutqvist et al., 2010; Court et al., 2012; Orlic and Wassing, 2013; Talebian et al., 2013; Wang and Peng, 2014; Wang et al., 2015). This numerical simulation is usually completed in two main stages, although the coupling of storage reservoir and caprock has been analyzed (Birkholzer et al., 2009; Zhou et al., 2015). The preliminary stage is to simulate the migration and interaction of the injected $CO_2$ with the storage

reservoir (Fan et al., 2012; Dalkhaa et al., 2013; Martinez et al., 2013; Saaltink et al., 2013; Jiang et al., 2014). The trapping mechanisms such as structural trapping, hydrodynamic trapping, solubility trapping, residual trapping, and mineral trapping are focused (Matter and Kelemen, 2009; Macminn et al., 2011; Kang et al., 2014). The plume formation and pressure build-up due to the $CO_2$ accumulation beneath the caprock layer are the outcomes (Hesse and Woods, 2010; Rutqvist et al., 2010; Golding et al., 2011; Boait et al., 2012; Zhao et al., 2012; Green and Ennis-King, 2013; Wang et al., 2014; Bielicki et al., 2015). The second stage is to investigate the migration of the accumulated $CO_2$ at the bottom of caprock and interaction between $CO_2$ and the caprock layer (Wang and Peng, 2014; Wang et al., 2015; Zhou et al., 2015). The focus at this stage is on the calculation of caprock sealing efficiency (Heath et al., 2012; Hou et al., 2012; Armitage et al., 2015). This sealing efficiency can be measured by many methods and the $CO_2$ penetration depth at the 1000th year is a good choice (IPCC, 2005).

Many numerical simulation tools have been developed to assess the $CO_2$ geological storage (Rutqvist and Tsang, 2002; Gherardi et al., 2007; Talebian et al., 2013; Wang and Peng, 2014; Andersen et al., 2015; Vilarrasa and Carrera, 2015). For instance, a fully coupled mathematical model was developed to simulate the multiphysical processes in the $CO_2$-brine displacement within a caprock layer (Anchliya et al., 2012; Wang and Peng, 2014). This model considers the mechanical deformation, the change of pore pressure, the alteration of gas sorption/desorption and the modification of geochemical reaction. Particularly, a two-phase flow model is proposed to describe the $CO_2$-brine displacement process in a fractured caprock layer. The movement of $CO_2$-brine front also induces local deformation of caprock, alters wettability and entry capillary pressure, and modifies the absolute or intrinsic permeability (Sadhukhan et al., 2012; Armitage et al., 2013; Farokhpoor et al., 2013; Wang and Peng, 2014). Therefore, the full coupling of these interactions may heavily affect $CO_2$ penetration depth or caprock sealing efficiency and should be fully taken into consideration. However, the computation of a fully coupled model is so complicated that it cannot be easily and fast implemented. A simple approach is necessary for a fast calculation of penetration depth.

One of simple approaches is the two-phase flow model for non-deformable porous medium. In the two-phase flow model, the $CO_2$-water-rock interaction is considered through capillary pressure. This capillary pressure can be affected by porosity, $CO_2$ state and rock properties (Wang and Peng, 2014; Li et al., 2015). This two-phase flow approach can be applicable for any dimensional problem. However, capturing the movement of $CO_2$-water front is a difficult task for the numerical simulations in both fully coupled model and two-phase flow model. The accumulated $CO_2$ spreads over the large area beneath the caprock bottom (Birkholzer et al., 2009; Bielicki et al., 2015), hence the penetration of $CO_2$ into the caprock layer can be simplified into one-dimensional (1D) problem. If the movement of $CO_2$-water front can be analytically solved, the calculation of penetration depth becomes an easy task. If the penetration is a diffusion process of an invading front into a semi-infinite medium, the concentration profile is described by a complementary error function (Crank, 1975; Murata et al., 2004; Matteo and Scherer, 2012). The penetration depth can be calculated by the square root law which refers to the square root of the product of diffusion coefficient and diffusion time. A similar expression is also obtained if the diffusion plus reaction rate is considered. Their difference is only the penetration speed and direction (Matteo and Scherer, 2012). In addition, the pressure difference between the pore pressure beneath the caprock (called injection pressure) and the initial pressure in the caprock layer (called reservoir pressure) may have significant impacts on the penetration depth. The above-mentioned diffusion-controlled process has difficulty in explicitly
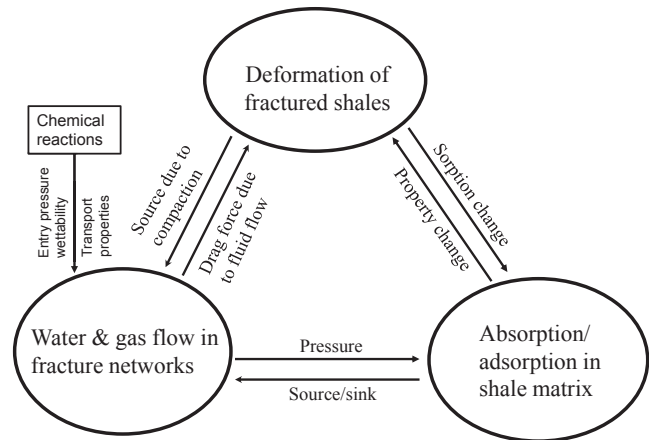


**Fig. 1.** Interactions of multiple processes within shale caprock.

expressing the effects of pressure magnitude and difference. Being different from the above-mentioned diffusion process, this study calculates the penetration depth through a seepage-controlled process. In this seepage-controlled process, the $CO_2$ pressure beneath the caprock and the pressure in the caprock layer can be easily taken into account.

A simple approach is proposed in this paper for a fast calculation of penetration depth. By using this approach, the penetration depth is explicitly expressed as the square root of pressure magnitude and difference. The effects of permeability and fluid mobility on penetration depth are explicitly expressed in the formula, too. This paper is organized as follows. First, the square root law is discussed by the numerical simulation results of fully coupled model and two-phase flow model. It is found that the square root law for time is still true even if sorption, swelling, deformation, and two-phase flow are all considered. Then, a simple model for fluid penetration is proposed based on the moving front seepage of an exotic fluid. This model deduces a moving front problem and the invading front of exotic phase or component is analytically solved. Third, the formula for the calculation of penetration depth is verified by three sets of experimental data taken from the literature. Finally, the analytical expression of penetration depth is extended to consider those factors affecting the fluid penetration such as compaction of fractured caprocks, sorption-induced swelling, and fluid property. It is demonstrated that this simple approach has the capability to describe the effect of pressure magnitude and difference on the penetration depth in the penetration process. The slope of the penetration depth versus time can comprehensively accumulate many factors and can be determined by fitting experimental data.

## 2. Square root law for time and pore pressure based on numerical simulations

Our numerical simulations have demonstrated that the multiphysical process interaction had some impacts on caprock sealing efficiency (Wang and Peng, 2014; Wang et al., 2015) and a linear relationship between penetration depth versus pressuring time and pressure magnitude was observed in the square root space. However, this square root law is slightly different for the fully coupled model and the two-phase flow model. Two-phase flow model describes a process without multiphysical process effect. It does not consider the geomechanical process, sorption and reaction process, and diffusion process in shale matrix. Therefore, the two-phase flow model cannot consider self-limiting (self-healing)/ self-enhancement and compaction phenomena. Fully coupled

model takes all of these effects into consideration and thus can describe the self-limiting/self-enhancement and compaction phenomena (Huerta et al., 2013; Wang and Peng, 2014). In this section, these two simulation models are briefed. Their simulations on 1D problem are compared and the linear relationship between penetration depth and square root of time is observed.

### 2.1. Fully coupled simulation model for multiphysical process interactions

This fully coupled model considering caprock is composed of fracture network and shale matrix. The caprock layer is sometimes called fractured caprock (Elkhoury et al., 2015). In the fracture network, the flow follows the Darcy's law, but in shale matrix, $CO_2$ follows a diffusion process. Its typical interactions shown in Fig. 1 include the following multiphysical processes: (1) mechanical deformation process; (2) two-phase flow process; and (3) $CO_2$-rock reaction. The geomechanical process, diffusion process, sorption process and reaction process are coupled in each time step (Wang and Peng, 2014; Wang et al., 2015). In this fully coupled model, thermal effect is neglected although the non-isothermal effects are important and were dealt with by some researchers (e.g. Vilarrasa et al., 2013; Goodarzi et al., 2015). Such a fully coupled model describes the phenomena of compaction, self-limiting, or self-enhancement (Wang and Peng, 2014). These processes are coupled through a suite of rock transport property models, including porosity model, permeability model, gas entry pressure model, gas sorption model, and swelling strain model. Their governing equations and constitutive models are listed below.

(1) Mechanical deformation

The mechanical deformation can be described by

$$Gu_{i,jj} + \frac{G}{1-2\nu}u_{k,kj} = K(\varepsilon_{s1,i} + \varepsilon_{s2,i}) - \alpha p_{,i} - f_i \tag{1}$$

where $u_i$ is the displacement in the $i$th direction; $f_i$ is the body force; $G$ and $\nu$ are the shear modulus and Poisson's ratio, respectively; $\alpha$ is the Biot's coefficient; $p$ is the pore pressure within shale; $K$ is the bulk modulus; $\varepsilon_{s1}$ is the sorption-induced volumetric strain; and $\varepsilon_{s2}$ is the chemical-reaction induced strain. In this study, no chemical reaction is considered, i.e. $\varepsilon_{s2} \equiv 0$.

(2) Two-phase flow in fracture network (no buoyancy considered here)

For water flow, we have

$$\phi C_p \frac{\partial p_{nw}}{\partial t} - \phi C_p \frac{\partial p_w}{\partial t} + S_w \frac{\partial \phi}{\partial t} = \nabla \cdot \left( \frac{kk_{rw}}{\mu_w} \nabla p_w \right) + \frac{f_w}{\rho_w} \tag{2}$$

For gas flow, we have

$$\phi'(S_{nw} - p_{nw}C_p)\frac{\partial p_{nw}}{\partial t} + \phi' p_{nw}C_p \frac{\partial p_w}{\partial t} + \phi S_{nw}p_{nw}\frac{\partial \phi}{\partial t}$$
$$= \nabla \cdot \left( \frac{kk_{rnw}}{\mu_{nw}} p_{nw} \nabla p_{nw} \right) - p_a \rho_c \frac{dm_b}{dt} + f_{nw} \tag{3}$$

The compressibility due to capillary pressure is

$$C_p = \frac{\partial S_w}{\partial p_c} = \frac{\partial S_w}{\partial S_w^*}\frac{\partial S_w^*}{\partial p_c} = (1 - S_{rw} - S_{rnw})\left[ -\frac{\lambda}{p_e}\left(S_w^*\right)^{1+\frac{1}{\lambda}} \right] \tag{4}$$

The alteration of porosity due to sorption is

$$\phi' = \phi + \rho_{ga}\rho_c\frac{V_L p_L}{(p_L + p)^2} \tag{5}$$

where $p_w$ and $p_{nw}$ are the pore pressures of water and $CO_2$ within the fracture network, respectively; $S_w$ and $S_{nw}$ are the degrees of saturation of water and $CO_2$, respectively; $S_w^*$ is the relative degree of saturation; $t$ is the real time; $k$ is the absolute permeability of the fractured caprock; $k_{rw}$ and $k_{rnw}$ are the relative permeabilities of water and $CO_2$ in the fracture network, respectively; $\mu_w$ and $\mu_{nw}$ are the viscosities of water and $CO_2$ at in-situ conditions, respectively; $\phi$ is the porosity of the fracture networks; $f_w$ and $f_{nw}$ are the sources of water and $CO_2$, respectively; $\rho_c$ and $\rho_w$ are the densities of caprock and water, respectively; $p_a$ is the standard atmospheric pressure; $m_b$ is the average remaining $CO_2$ content in the shale matrix; $S_{rw}$ and $S_{rnw}$ are the residual degrees of saturation of water and $CO_2$, respectively; $\lambda$ is the heterogeneous index; $p_e$ is the entry capillary pressure; $p_c$ is the capillary pressure ($p_c = p_{nw} - p_w$); $\rho_{ga}$ is the gas density at the pressure $p_a$; $V_L$ is the Langmuir volume; $p_L$ is the Langmuir pressure; and $p = p_w S_w + p_{nw}S_{nw}$.

(3) Diffusion in matrix

The diffusion in matrix can be written as

$$\frac{dm_b}{dt} = -\frac{1}{\tau}[m_b - m_e(p)] \tag{6}$$

where $\tau$ is the diffusion time, and $m_e(p)$ is the $CO_2$ content in the shale matrix when the pore pressure within shale matrix is equal to the pore pressure $p$ in the fracture network.

These governing equations are coupled through the following transport property models:

(1) Porosity model (Wang et al., 2013)

$$\frac{\phi}{\phi_0} = 1 + (1 - R)\Delta\varepsilon_e \tag{7}$$

where $\phi_0$ is the initial porosity, $\Delta\varepsilon_e$ is the increment of effective volumetric strain. For homogeneous porous medium, $R$ can be roughly expressed as $R = \alpha/\phi_0$.

(2) Permeability model

$$\frac{k}{k_0} = \left(\frac{\phi}{\phi_0}\right)^3 \tag{8}$$

where $k_0$ is the initial permeability.

(3) Relative permeability model

$$\left. \begin{aligned} k_{rw} &= k_{rw}^{max}\left(S_w^*\right)^{N_w} \\ k_{rnw} &= k_{rCO_2}^{max}\left(S_{CO_2}^*\right)^{N_{CO_2}} \end{aligned} \right\} \tag{9}$$

where $k_{rw}^{max}$ and $k_{rCO_2}^{max}$ are end-point relative permeabilities for water and $CO_2$, respectively; $N_w$ and $N_{CO_2}$ are the fitting constants for relative permeabilities of water and $CO_2$, respectively; $S_{CO_2}^*$ is the relative degree of saturation of $CO_2$, and $S_{CO_2}^* + S_w^* = 1$.

(4) Capillary pressure model

$$S_w^* = \left(\frac{p_e}{\gamma p_c}\right)^\lambda \tag{10}$$

where $\gamma$ is a constant.

(5) Entry capillary pressure model

$$p_e = \frac{p_{ei}}{1 + B\Delta\varepsilon_e} \tag{11}$$

where $p_{ei}$ is the initial entry capillary pressure, and $B$ is a constant.

(6) Langmuir isotherm in shale matrix (Li and Elsworth, 2014)

$$m_b = \frac{V_{Lm}p_m}{p_{Lm} + p_m} \tag{12}$$

where $p_m$ is the pore pressure in shale matrix; $V_{Lm}$ and $p_{Lm}$ are the Langmuir volume constant and Langmuir pressure for shale matrix, respectively.

(7) Swelling strain of shale matrix

$$\varepsilon_{s1} = \frac{\varepsilon_{Lm}p_m}{p_{Lm} + p_m} \tag{13}$$

where $\varepsilon_{Lm}$ is the Langmuir strain of shale matrix.

This fully coupled finite element model simultaneously solves both pore pressure and displacement of caprock. It employs an iterative algorithm to satisfy the nonlinear formulations due to two-phase flow and gas sorption-induced evolution of porosity and permeability, and alteration of entry capillary pressure within the given tolerance of errors. This approach incorporates the evolutions of various physical and transport properties, including (a) shale porosity as defined by Eq. (7), (b) absolute permeability as defined by Eq. (8), (c) relative permeability as defined by Eq. (9), (d) capillary pressure as defined by Eq. (10), (e) gas entry pressure as defined by Eq. (11), (f) gas adsorption as defined by Eq. (12), and (g) sorption-induced matrix swelling strain as defined by Eq. (13).

## 2.2. Two-phase flow model

When geomechanical deformation, sorption and reaction process, and diffusion process in shale matrix are all ignored, this fully coupled model is simplified into a two-phase (water and $CO_2$) flow model. At this time, $\partial\phi/\partial t = 0$, porous medium is rigid, thus Eqs. (2) and (3) become the following governing equations.

For water flow, we have

$$\phi C_p \frac{\partial p_{nw}}{\partial t} - \phi C_p \frac{\partial p_w}{\partial t} = \nabla\cdot\left(\frac{kk_{rw}}{\mu_w}\nabla p_w\right) + \frac{f_w}{\rho_w} \tag{14}$$

For gas flow, we have

$$\phi\left(S_{nw} - p_{nw}C_p\right)\frac{\partial p_{nw}}{\partial t} + \phi p_{nw}C_p\frac{\partial p_w}{\partial t}$$
$$= \nabla\cdot\left(\frac{kk_{rnw}}{\mu_{nw}}p_{nw}\nabla p_{nw}\right) + f_{nw} \tag{15}$$

This is a two-phase flow model. It describes the interaction between $CO_2$ and water in rigid porous media. The interfacial tension and capillary pressure can be still incorporated into this model, but no interaction with rock deformation is involved.

## 2.3. Comparison of fully coupled model and two-phase flow model

Both two-phase flow and fully coupled models are applied to 1D problem as shown in Fig. 2. Because this is 1D problem, only 10 m in side length of the model is sufficient. The $CO_2$ is accumulated at the bottom of the caprock layer and its pore pressure can be pre-specified. Table 1 lists all parameters used in the simulations for both the fully coupled model and the two-phase flow model. Fig. 3a presents the change of penetration depth with real time before gas breakthrough. It is observed that these two curves are different. The penetration depth for two-phase flow model is much larger. Their difference of penetration depth becomes larger with pressuring time. This difference may come from sorption process. Detailed numerical simulations reveal that the sorption and reaction of $CO_2$/rock retards the penetration speed. This thus causes fully coupled model to have much smaller penetration depth. It is noted that after $CO_2$ breakthrough, some substances may be washed away and the self-enhancement mechanism may be activated (Matteo and Scherer, 2012; Huerta et al., 2013). It is also noted that self-healing mechanisms may occur due to chemical reactions and shale ductility (Noiriel et al., 2004; Matteo and Scherer, 2012). All of these factors are included in the above simulation, but a square root law is still observed in the relationship between penetration depth and time. Fig. 3b replots this relationship in the domain of time square root. Both two-phase flow model and fully coupled model follow a straight line but with different slopes. This difference of slopes is determined by multiphysical interactions. Therefore, a square root law is applicable to the relationship of penetration depth and time for these two models but the determination of this square root law depends on the interaction among multiphysical processes.

## 3. A simple model for fast calculation of exotic phase penetration

The above two-phase flow model can be further simplified into a seepage-controlled model if the capillary pressure between $CO_2$ and brine is ignored. Fig. 4 presents a typical seepage-controlled model with moving invading front, which is a 1D penetration
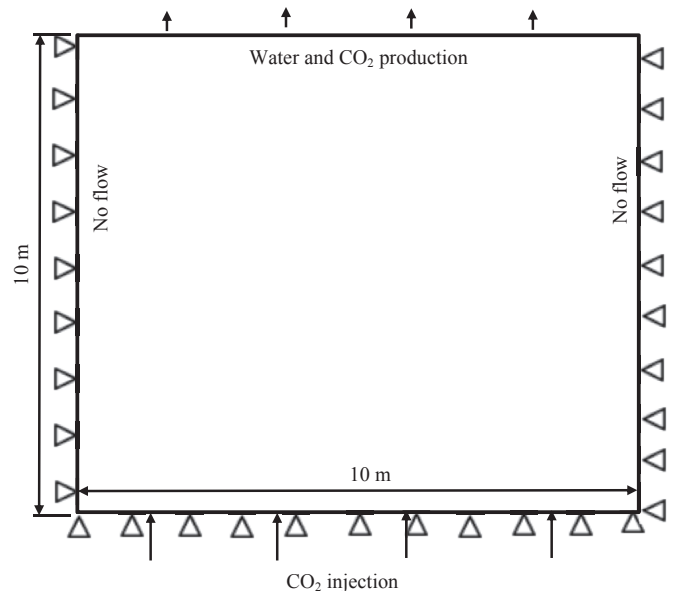


**Fig. 2.** Computational model for $CO_2$-water displacement.

**Table 1**
Model parameters used in computation.

| Parameter | Unit | Value | Physical meanings |
|---|---|---|---|
| $S_{nwr}$ | | 0.15 | Residual degree of saturation of $CO_2$ |
| $S_{wr}$ | | 0.6 | Residual degree of saturation of water |
| $P_{ei}$ | MPa | 10 | Initial capillary entry pressure |
| $\mu_w$ | Pa s | $3.6 \times 10^{-4}$ | Water viscosity at pressure of 19 MPa and temperature of 353.15 K or 80 °C |
| $\mu_{nw}$ | Pa s | $5.2 \times 10^{-5}$ | $CO_2$ viscosity at pressure of 19 MPa and temperature of 353.15 K or 80 °C |
| $\lambda_w$ | | 6.5 | Corey parameter for water |
| $\lambda_{nw}$ | | 2.6 | Corey parameter for $CO_2$ |
| $\lambda_0$ | | 2 | Pore size distribution index |
| $p_{wf}$ | MPa | 8.95 | Pressure at the top boundary |
| $p_{w0}$ | MPa | 8.95 | Initial water pressure in caprock |
| $p_{nw0}$ | MPa | 19 | Initial $CO_2$ pressure in caprock |
| $T$ | K | 353.15 | Temperature ($CO_2$ storage reservoirs are likely to be 338 K–358 K or higher) |
| $k_0$ | $m^2$ | $1.5 \times 10^{-19}$ | Initial absolute permeability |
| $\phi_0$ | | 0.04 | Initial porosity |
| $p_L$ | MPa | 6 | Langmuir pressure of $CO_2$ in shale |
| $V_L$ | $m^3\ kg^{-1}$ | 0.03 | Langmuir sorption capacity of shale for $CO_2$ |
| $E_c$ | GPa | 8 | Young's modulus of shale |
| $E_s$ | GPa | 20 | Young's modulus of shale grains |
| $\nu$ | | 0.3 | Poisson's ratio of shale |
| $\rho_c$ | $kg\ m^{-3}$ | 2300 | Shale density |
| $p_{gout}$ | MPa | 19 | $CO_2$ pressure at the top boundary |
| $p_{wout}$ | MPa | 8.95 | Water pressure at the top boundary |
| $\lambda$ | | 0 | Parameter for $CO_2$ entry pressure |
| $D$ | $m^2\ s^{-1}$ | $1.2 \times 10^{-11}$ | Diffusion coefficient of shale matrix (variable with diffusion time) |
| $k_{rw}^{max}$ | | 1 | End-point relative permeability for water phase |
| $k_{rCO_2}^{max}$ | | 0.015 | End-point relative permeability for $CO_2$ phase |





**Fig. 3.** Comparisons of penetration depth for two-phase flow model and fully coupled model. (a) Penetration depth with time. (b) Penetration depth with time square root.

problem. Our model assumes that the penetration front coincides with the pressure distribution front of the injected fluid. This is true for exotic phase because the $CO_2$ concentration coincides with pressure. In this figure, pressure $p_1$ is applied along the inlet boundary of the caprock (we call it as an injection pressure for the caprock). The initial pressure in the caprock (we call this pressure as reservoir pressure) is $p_2$. The pressure difference ($=p_1 - p_2$) between injection pressure and reservoir pressure drives the injected fluid to further penetrate into the caprock. The calculation of penetration depth $H$ is still focused. This depth refers to the distance between the invading front (dashed line) and the inlet boundary. This penetration depth can be obtained based on the Darcy's law below.

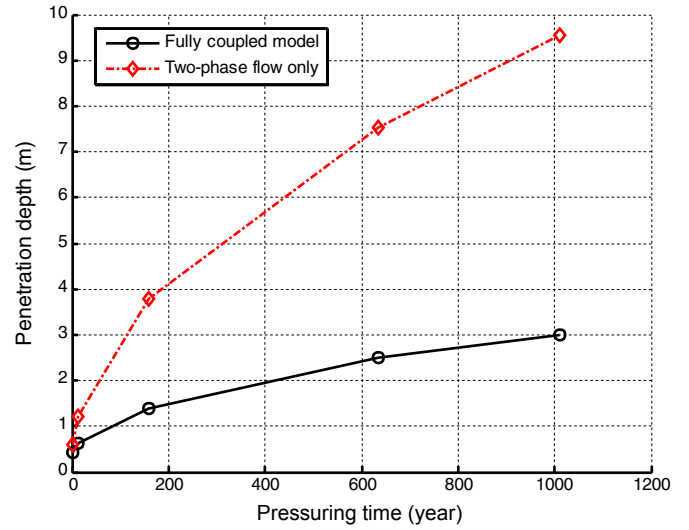The speed of the invading front is

$$u_H = \frac{dH}{dt} \tag{16}$$

The Darcy's velocity at the front is

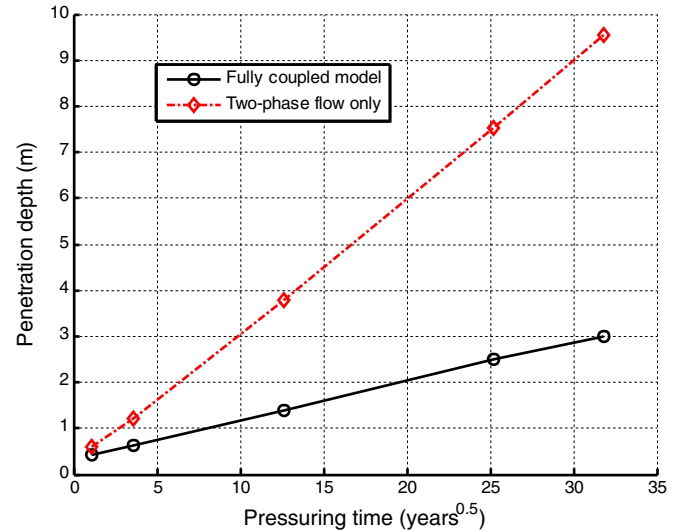$$u_x|_{x=H} = -\frac{k}{\mu}\frac{\partial p}{\partial x}\bigg|_{x=H} \tag{17}$$

Both velocities should be equal at the front, thus we have

$$\frac{dH}{dt} = -\frac{k}{\mu}\frac{\partial p}{\partial x}\bigg|_{x=H} \tag{18}$$

where $\partial p/\partial x|_{x=H}$ is determined by the fluid flow in porous media. This is a 1D flow problem with moving boundary. For this seepage problem, if the time-dependent term is ignored, the conservation law of mass is approximated by

$$\frac{\partial}{\partial x}\left(-\rho\frac{k}{\mu}\frac{\partial p}{\partial x}\right) = 0 \tag{19}$$

Its boundary conditions are

$$p = \begin{cases} p_1 & (x = 0) \\ p_2 & (x = H) \end{cases} \tag{20}$$

For incompressible fluid, the solution to Eq. (19) is

$$p = \frac{p_2 - p_1}{H}x + p_1 \tag{21}$$

and

$$\frac{\partial p}{\partial x}\bigg|_{x=H} = \frac{p_2 - p_1}{H} \tag{22}$$

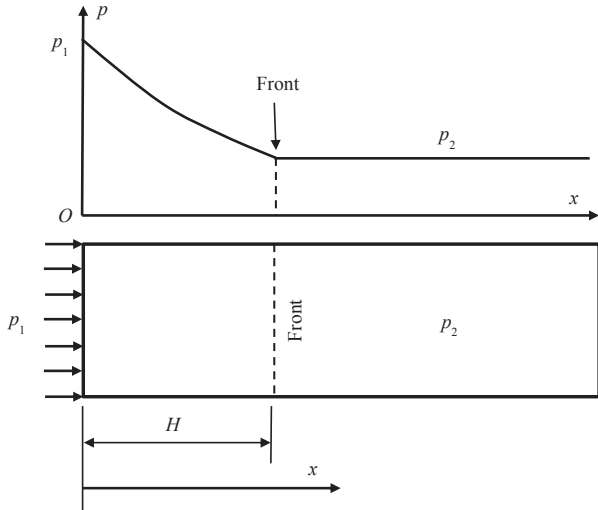The equation for the front movement is thus obtained as

**Fig. 4.** Fluid penetration into reservoirs.

$$\frac{\mathrm{d}H}{\mathrm{d}t} = -\frac{k}{\mu}\frac{p_2 - p_1}{H} \tag{23}$$

The penetration depth $H$ is then calculated by

$$H = \sqrt{\frac{2kt}{\mu}(p_1 - p_2)} \tag{24}$$

For an ideal compressible gas, the gas density is $\rho = Ap$, where $A$ is assumed to be a constant. Therefore, the pressure distribution follows a parabolic curve as

$$p^2 = \frac{p_2^2 - p_1^2}{H}x + p_1^2 \tag{25}$$

and

$$\left.\frac{\partial p}{\partial x}\right|_{x=H} = \frac{p_2^2 - p_1^2}{H}\frac{1}{2p_2} \tag{26}$$

Again, we have

$$\frac{\mathrm{d}H}{\mathrm{d}t} = -\frac{k}{\mu}\left.\frac{\partial p}{\partial x}\right|_{x=H} = \frac{k}{\mu}\frac{p_1^2 - p_2^2}{H}\frac{1}{2p_2} \tag{27}$$

The penetration depth is

$$H = \sqrt{\frac{kt}{\mu}\frac{p_1^2 - p_2^2}{p_2}} = \sqrt{\frac{2kt}{\mu}(p_1 - p_2)}\sqrt{\left(1 + \frac{p_1}{p_2}\right)\bigg/2} \tag{28}$$

It is noted that the penetration depth by either Eq. (24) or Eq. (28) increases with the square root of time $t$ and the pressure difference $(p_1 - p_2)$. The penetration speed is significantly affected by the flow mobility $k/\mu$ in porous media. Under the same pressure difference, penetration depth is larger for higher mobility fluid. For a compressible fluid, this flow mobility is amplified by $(1 + p_1/p_2)/2$. This implies that the penetration speed for compressible fluid depends on not only the pressure difference but also the ratio of their magnitudes. This makes the effect of pressure difference vary with burial depth. At shallower depth, the ratio is larger and thus the penetration depth is larger. At deeper depth, this ratio becomes smaller and the amplification effect becomes weaker. In addition, permeability and its evolution can express the effects of many

factors (to be discussed in Section 5). Therefore, any mechanical or chemical actions can be taken into account only through the evolution of permeability. In addition, $CO_2$ may be non-ideal gas in the penetration process. Eq. (28) will be slightly modified based on the compressibility of $CO_2$ (such as Vilarrasa et al., 2010). This study still assumes that Eq. (28) is applicable but the coefficient can be calibrated with the square root law through laboratory or field data.

## 4. Comparison with experimental observations

This section will check the applicability of the above formulae for the calculation of penetration depth by three sets of experimental data. The square root laws for pressure and time are verified respectively through two tests on water penetration into concrete and one penetration test of hydrochloric acid and carbonic acid into cement. Although water penetration into concrete is different from the $CO_2$ permeation into shale caprock in micro-flow mechanisms, such a check is still meaningful for the proposed simple approach.

### 4.1. Test #1

Murata et al. (2004) conducted a seepage test to investigate the watertightness of concrete. They tested three samples which were prepared with three water-cement ratios ($w/c$) of 0.55, 0.7 and 0.8, respectively. They used photographs to measure the penetration depth of water with pressuring time. The injected fluid was water, thus being almost incompressible. Therefore, Eq. (24) is used to fit these experimental data. Fig. 5 is the fitting result for the relationship between penetration depth and injection pressure (water). The penetration depth was measured for a test period (pressuring time) of 48 h. This figure shows that Eq. (24) well fits these experimental data of three concrete samples. The relationship between penetration depth and injection pressure observes a square root law.

At a fixed injection pressure, Eq. (24) shows that the penetration depth increases with pressuring time. This equation is again used to fit the relationship between penetration depth and pressuring time for the three samples. The fitting results are presented in Fig. 6a for $w/c = 0.55$, in Fig. 6b for $w/c = 0.7$, and in Fig. 6c for $w/c = 0.8$. These figures show that the square root law is applicable for the relationship of penetration depth and pressuring time. They also show
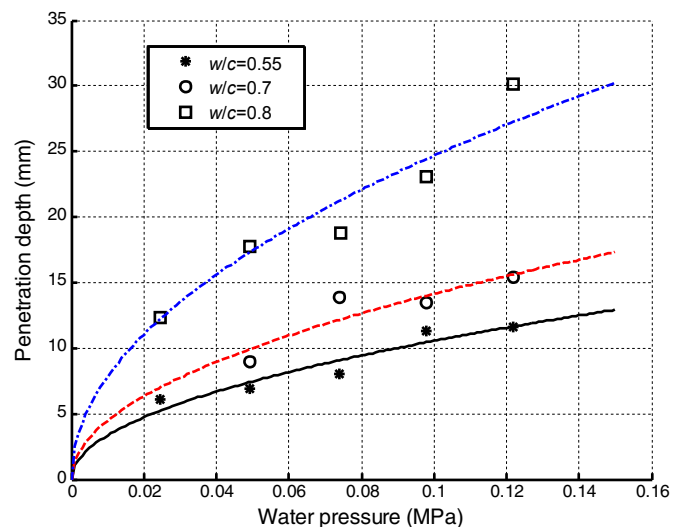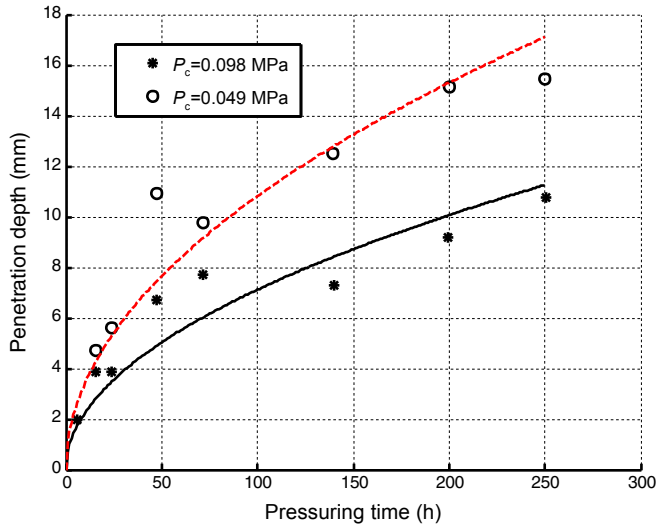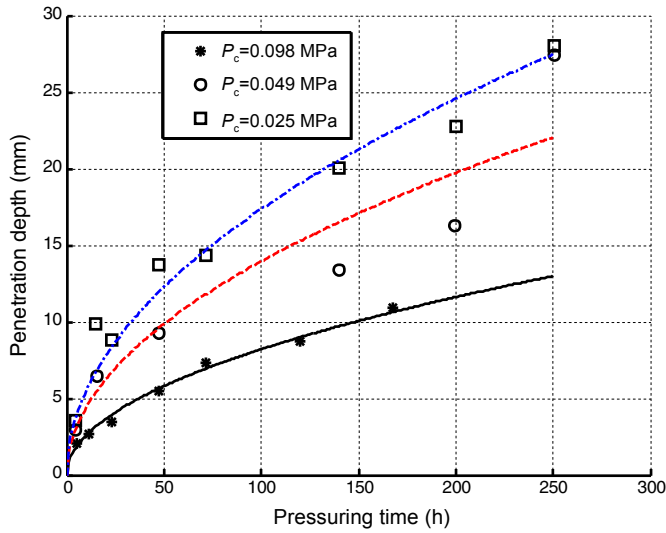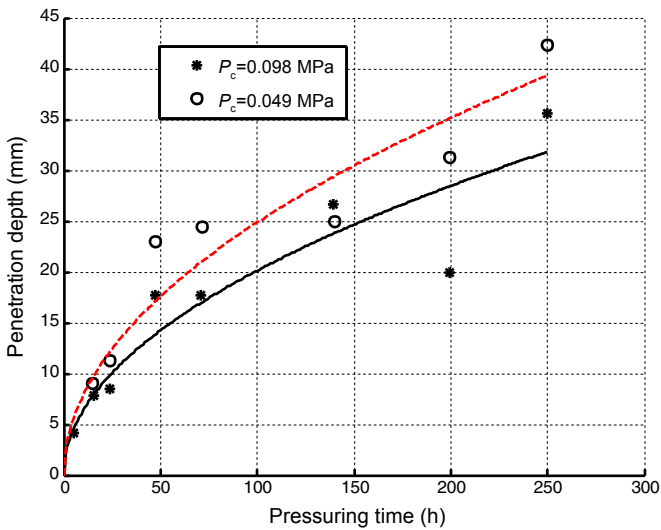


**Fig. 5.** Relationship of penetration depth and water pressure (Lines: Fitted by Eq. (25); Symbols: Experimental data).

(a)



(b)



(c)

**Fig. 6.** Relationships of penetration depth and pressuring time (Lines: Fitted by Eq. (25); Symbols: Experimental data). (a) Water-cement ratio = 0.55. (b) Water-cement ratio = 0.7. (c) Water-cement ratio = 0.8.

that the sample under higher confining pressure ($P_c$) has lower penetration depth. Under higher confining pressure, the sample is denser, thus lower intrinsic permeability and smaller penetration depth were obtained. Further, the water-cement ratio has significant impacts on the penetration depth. Higher water-cement ratio means that the concrete has higher permeability, hence the penetration depth is higher. As a summary, the relationship of penetration depth and pressuring time follows the square root law. The external force induced compaction and the initial status of the concrete sample affect the penetration depth. Higher confining pressure causes lower penetration depth. Lower ratio of water to cement induces lower penetration depth, too.

### 4.2. Test #2

This is another test to investigate the watertightness of concrete. Being different from the Test #1, Yoo et al. (2011) tested three samples with uniaxial compressive strength ($\sigma_c$) of 16 MPa, 21 MPa, and 27 MPa, respectively and obtained a set of experimental data under the injection pressure of 1.5 MPa. The penetration depths of three samples were measured at the pressuring time of 48 h, 96 h, 144 h and 192 h, respectively. Because the injected fluid is water, Eq. (24) is still used to fit these experimental data. Fig. 7 is the fitting result for the relationship of penetration depth and pressuring time for the three samples. This figure shows that the square root law is applicable to the relationship of penetration depth and time regardless of concrete strength. Higher strength has lower penetration depth. This may be because the sample with higher strength has lower permeability. Again, the square root law is observed for pressuring time for the three samples with different strengths.

### 4.3. Test #3

Matteo and Scherer (2012) conducted a test to investigate the penetration of hydrochloric acid and carbonic acid into Class H Portland cement. Being different from the above two tests, they also performed flow-through tests using 1 M HCl over a range of flow rates from 7.5 mL/h to 300 mL/h. Such a test was designed to check the effect of geochemical reaction on penetration depth. This test obtained a complete penetration process under the pressuring time
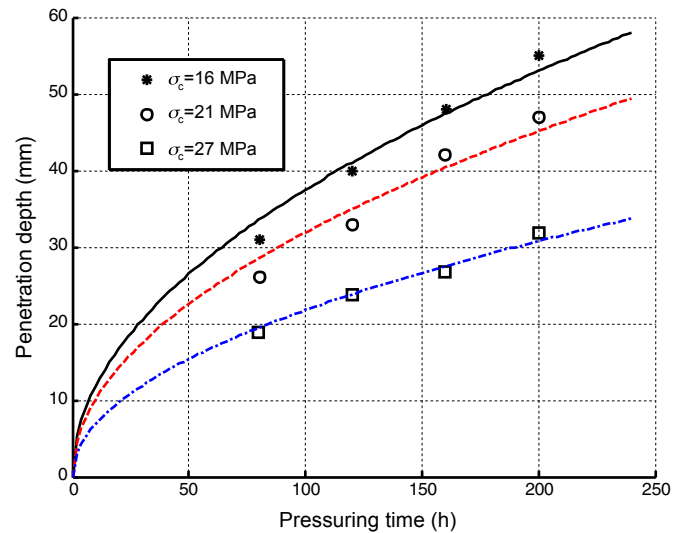


**Fig. 7.** Relationships of penetration depth and pressuring time for concrete samples with different uniaxial compressive strengths (Lines: Fitted by Eq. (24); Symbols: Experimental data).

up to 50 h. Eq. (24) is still used to fit the relationship of penetration depth and time. The fitting result is shown in Fig. 8. This figure shows that Eq. (24) well fits these experimental data. In addition, the penetration tests were conducted in different directions to identify the anisotropy of flow path. The upright direction has much lower permeability, thus the penetration depth in this direction is much smaller. This figure also shows that lower flow rate has slightly less penetration depth. Flow rate has slight impact on penetration depth. This impact may be due to dissolution or deposition mechanisms from acid-brine-rock interaction in flow-through tests. These results imply that geochemical reaction within caprock affects penetration depth or caprock sealing efficiency. This process may have some self-limiting or self-enhancement mechanism depending on flow pattern. For this $CO_2$-brine-rock interaction problem, a fully coupled model is necessary to consider all of these mechanisms.

## 5. Analysis for those factors affecting $CO_2$ penetration

This simple formula of Eq. (24) or (28) shows that the penetration depth still follows the square root law of permeability. Fig. 9 is a typical relationship between $CO_2$ penetration depth at the time of 317 years and absolute permeability. This curve was obtained by our fully coupled model with the parameters in Table 1 as the base parameters. Only intrinsic permeability is changed from $1.5 \times 10^{-21}$ m$^2$ to $1.5 \times 10^{-17}$ m$^2$. The computational model is 10 m wide and 30 m high. Other conditions are the same as Fig. 2. Fig. 9 shows that the effect of permeability on penetration is complex. It may not follow the square root law. This section will investigate those factors affecting permeability evolution such as compaction, sorption-induced swelling, capillary pressure, and fluid transport property. Through these analyses, the simple formula of Eq. (24) or (28) is extended in its application range.

### 5.1. Compaction-induced permeability change of fractured caprock

As discussed in Section 3, this simple approach shows that penetration depth depends on permeability and its evolution. For a fracture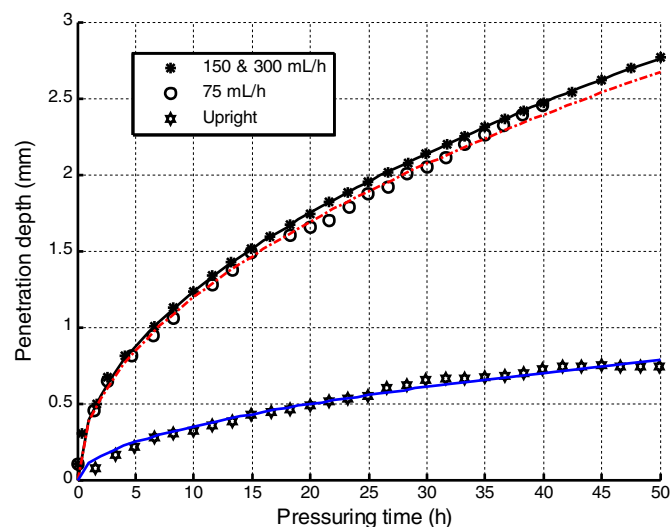d caprock, its permeability has two components: fracture permeability and matrix permeability. Thus, the total permeability of this fractured caprock is expressed as

$$k = k_m + k_f = k_f\left(1 + k_m\big/k_f\right) \tag{29}$$

where $k_m$ is the matrix permeability, and $k_f$ is the fracture permeability. The matrix permeability $k_m$ is much smaller than the fracture permeability $k_f$, i.e. $k_f > 100k_m$, thus one can have an approximation as

$$k \approx k_f \tag{30}$$

Fractured caprock will change its compressibility under compaction. Both fracture and matrix contribute to this change of compressibility. If the contribution from matrix is ignorable, the compressibility coefficient of the fractured caprock can be expressed as

$$c_f = -\frac{1}{\phi_f}\frac{\partial \phi_f}{\partial \sigma_e} \tag{31}$$

where $\phi_f$ is the porosity of fracture, and $\sigma_e$ is the effective stress on the fracture network. Because of nonlinearity of fracture deformation (Barton, 2013; Zhang, 2013; Rutqvist, 2015), constant fracture compressibility is not suitable for a large range of stress change. If the cubic law for fracture flow is true and fracture compressibility observes an exponential function, the permeability-stress relationship can be assumed to follow an exponential function as (Briggs et al., 2014; Ma, 2015):

$$k = k_0 \exp\left[-3c_f(\sigma_e - \sigma_{e0})\right] \tag{32}$$

where $\sigma_{e0}$ is the initial effective stress on the fracture network. If the caprock is under uniaxial strain condition and its overburden stress remains unchanged during $CO_2$ penetration, the permeability of fracture network is then expressed as the function of pore pressure only:

$$k = k_0 \exp\left[3c_f\frac{\nu}{1-\nu}\alpha_B(p - p_0)\right] \tag{33}$$

where $\alpha_B$ is the material constant and $p_0$ is the initial pore pressure. Obviously, the compaction-induced change of permeability is directly linked to the change of pore pressure at that point. This result is obtained at the assumption of constant total stress. This assumption is similar to that of P&M model for coalbed methane extraction (Palmer and Mansoori, 1998). Eq. (33) directly links the change of permeability with the increment of pore pressure. For rigorous porous media, $c_f \approx 0$ and $k$ is constant. No compaction effect can be considered.

### 5.2. Two-phase flow

This simple approach does not consider the capillary pressure in $CO_2$-water flow. Two-phase flow in porous media has a key parameter of capillary pressure $p_c$. If the injection pressure is less than entry capillary pressure (Watts, 1987), the $CO_2$-water interface does not penetrate into the shale layer. Otherwise, a progressive penetration of $CO_2$ into the shale layer can be observed. For such a penetration problem, this simple approach is slightly modified to consider the effect of capillary pressure. Capillary pressure is to balance the interfacial tension between $CO_2$ and water, thus it has no contribution to the driving force to the viscous fluid flow in porous medium. So the capillary pressure should be taken away from the pressure difference. For example, the pressure $p_1$ should
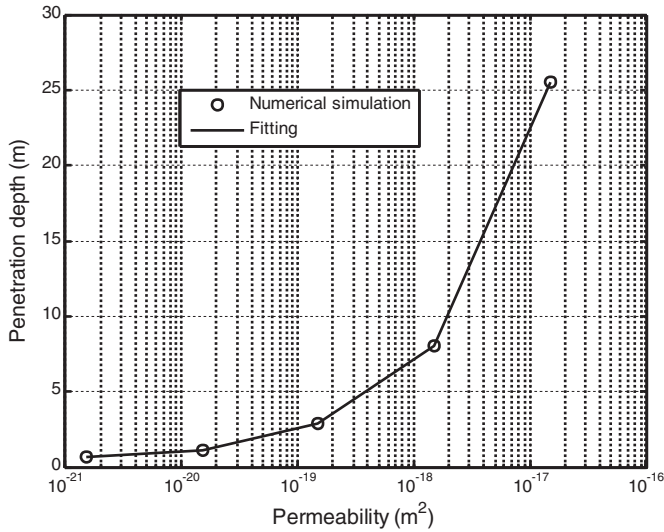


**Fig. 8.** Relationships of pressuring time and penetration depth for concrete samples with different uniaxial compressive strengths (Lines: Fitted by Eq. (24); Symbols: Experimental data).

**Fig. 9.** Increase of penetration depth with increase of absolute permeability.

be reduced to a new $p'_1(p'_1 = p_1 - p_c)$. The pressure difference between $p'_1$ and $p_2$ is the driving force to the viscous flow of $CO_2$. Eq. (28) is still applicable after the replacement of $p_1$ with $p'_1$:

$$H = \sqrt{\frac{2kt}{\mu}(p'_1 - p_2)}\sqrt{\left(1 + \frac{p'_1}{p_2}\right)\Big/2} \qquad (34)$$

### 5.3. Fluid state (gas or liquid) (viscosity and density)

The thermodynamic parameters of fluid, particularly the viscosity and compressibility of fluid, change with temperature ($T$) and pressure ($p$). The changes are more sensitive whether the $CO_2$ flow is in gaseous or supercritical state. Its thermodynamics changes both fluid mobility and storage capacity in pore space, thus altering the penetration speed. Both density and viscosity can be calculated by the equation of state such as Peng-Robinson equation (Peng and Robinson, 1976). This simple approach can take this change into account through the modification of fluid mobility in porous medium. At the same temperature and a small range of pressure change, the thermodynamics of fluid can be regarded as constants.

### 5.4. Sorption-induced swelling and fracture-matrix interaction

Shale matrix will swell after the adsorption of $CO_2$ if the $CO_2$ infiltrates into the shale matrix. Again, the infiltration into shale matrix can be assumed to follow a diffusion process and be associated with the magnitude of pore pressure. This infiltration induced swelling strain $\varepsilon_v$ is then expressed as

$$\varepsilon_v = \varepsilon_{v0}\{1 - \exp[-D(t - t_0)]\} \qquad (35)$$

where $t_0$ is the time at start point, and the initial swelling strain $\varepsilon_{v0}$ can be expressed by

$$\varepsilon_{v0} = \varepsilon_{Lm}\left(\frac{p}{p + p_{Lm}} - \frac{p_0}{p_0 + p_{Lm}}\right) \qquad (36)$$

If the total volumetric strain for the shale caprock is constant, this swelling of shale matrix occupies the flow channels of fracture network and thus changes the permeability of fractured caprock as below.

For self-limiting, we have

$$k = k_0\{1 - \exp[-D_k(t - t_0)]\} \qquad (37)$$

For self-enhancement, we have

$$k = k_0\{1 - \{1 - \exp[-D_k(t - t_0)]\}\} \qquad (38)$$

where $D_k$ is a swelling diffusion coefficient which is closely related to the diffusion coefficient $D$. For such a fracture-matrix system with constant total volume, its permeability is evolving as

$$k_0 = k_{0i}\left[1 - R_f\varepsilon_{Lm}\left(\frac{p}{p + p_{Lm}} - \frac{p_0}{p_0 + p_{Lm}}\right)\right]^3 \qquad (39)$$

where $k_{0i}$ is the initial permeability without swelling, and $R_f$ is a constant related to fracture spacing, aperture and fracture length in a representative element volume (Wang et al., 2015).

### 5.5. Performance of this extended simple approach

The above-extended simple formula of Eq. (28) includes compaction, sorption-induced swelling and fluid state. Its performance is demonstrated here. In the calculation, only one parameter is changed and all other parameters are kept constant. Fig. 10a presents the effect of compaction on penetration depth. Because the compaction process is completed at the beginning of penetration, this compaction affects only its initial permeability. Obviously, compaction changes the slope of square root curve of penetration depth versus time. It is again observed that smaller initial permeability corresponds to smaller penetration depth. Fig. 10b presents the effect of burial depth on penetration process under the same injection pressure. These curves are obtained under the same initial permeability, the same injection pressure but at different burial depths (expressed by the initial pore pressure in the caprock layer). This figure shows that larger burial depth corresponds to less penetration depth. This observation is true even if the pressure difference (or overpressure) is kept the same at different burial depths (see Fig. 10c). Of course, Fig. 10b and c shows that the overpressure is the main factor. Finally, swelling strain due to mass loss can be described in this simple formula. Fig. 10d compares the behaviors of constant permeability, increasing permeability (self-enhancement) and decreasing permeability (self-limiting) due to swelling strain. This is in agreement with those observations by Matteo and Scherer (2012). The self-enhancement is strong at the initial stage and gradually becomes weak and stable. This is because the mass loss is stronger at the beginning and gradually vanishes with time in flow-through tests. Such a process can be expressed through the change of volumetric strain. However, the self-limiting is weaker at the initial stage and gradually becomes stronger. This is because reaction or sorption-induced swelling needs time for contacting and infiltration into shale matrix. Therefore, such a simple approach can fast estimate the penetration depth although some mechanisms cannot be identified. Very important issue is that this formula can be calibrated by some initial data in laboratory or field measurements without knowing the properties of caprock. This makes the formula practicable.

## 6. Conceptual zoning for caprock sealing efficiency

The above assessment of caprock sealing efficiency can be drawn with a conceptual zoning in Fig. 11, where the injection pressure is expressed in a square root domain and the limit injection pressure refers to the maximum accumulated pressure beneath the caprock layer (Green and Ennis-King, 2013). This plot is drawn based on
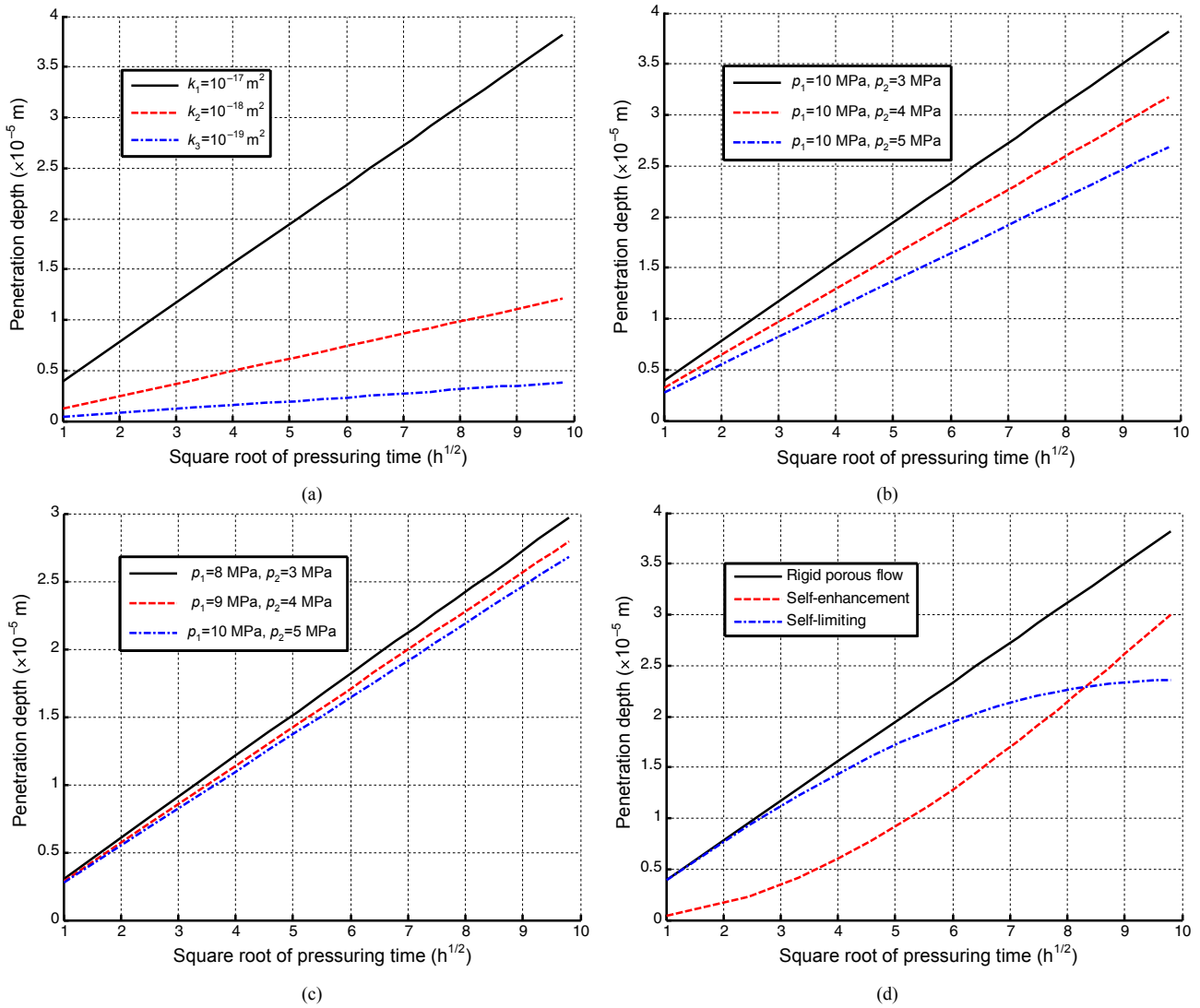
**Fig. 10.** Increase of penetration depth with increase of pressuring time. (a) Compaction effect. (b) Effect of burial depth under the same injection pressure. (c) Effect of burial depth under the same overpressure. (d) Self-limiting and self-enhancement behaviors.
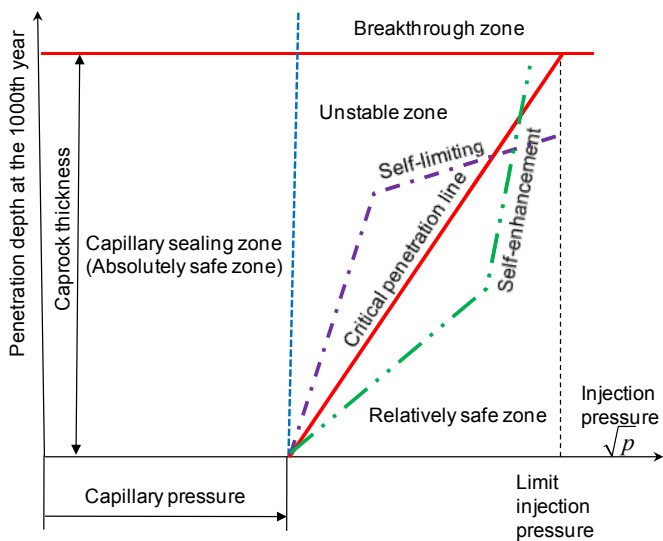


**Fig. 11.** Conceptual zoning for caprock sealing efficiency.

(entry) capillary pressure, square root law and potential interactions. As shown in Fig. 11, the whole domain is divided into capillary sealing zone, relatively safe zone, unstable zone, and breakthrough zone. When injection pressure is smaller than entry capillary pressure, no $CO_2$-brine displacement is activated and the caprock sealing is absolutely safe for volumetric (Darcy) flow. This zone is called capillary sealing zone. Between this pressure and limit injection pressure, the $CO_2$-brine displacement has been activated. The $CO_2$ front is continuously moving inward with injection pressure and the penetration depth is increasing correspondingly. When the penetration depth reaches its limit or caprock thickness, the caprock layer is breakthrough. At this time, $CO_2$ flow-through phenomena are observed and the caprock sealing is in the breakthrough zone. After breakthrough, some mechanisms particularly for self-enhancement may be activated (Huerta et al., 2013). Thus the caprock layer in this breakthrough zone is at risk.

The relative safe zone and unstable zone form a multiphysical interaction zone. This zone is adjacent to capillary sealing zone, breakthrough zone and bounded by the limit injection pressure. Multiphysical interaction may occur in this zone and affect the evolution of penetration process. According to the square root law, a straight critical penetration line divides this zone into relatively

safe zone and unstable zone. In the relatively safe zone, the $CO_2$ front cannot penetrate through the caprock layer and enter into the breakthrough zone if the current conditions do not change. In the unstable zone, a breakthrough can be expected under current conditions. However, this critical penetration line can be crossed through the activation of new mechanisms such as self-limiting or self-enhancement. For example, a process is in the relatively safe zone at the beginning, but some self-enhancements may be activated. This makes further penetration cross the line. The similar phenomenon can be observed in the unstable zone. Similar phenomena have been experimentally observed by Matteo and Scherer (2012). They observed self-limiting for the inverted case (no flow-through case) and self-enhancement for the 7.5 mL/h case (a flow-through case). Therefore, key issues for the assessment of caprock sealing efficiency are to determine this critical penetration line and to identify potential mechanisms of either self-limiting or self-enhancement through either tests or numerical simulations. The fully coupled model is a good tool for the solution of these key issues but further investigations are necessary to fully understand the interactions of multiphysical processes with updated geological and experimental data. The simple approach in this paper can help to explore potential mechanism transition and predict the potential breakthrough time if the current conditions are not changed.

## 7. Conclusions

This study proposed a simple approach to fast calculate the penetration depth of $CO_2$-water front in a saturated caprock layer. The formula based on this simple approach is then verified by three sets of experimental data for concrete samples as well as a fully coupled numerical model and a two-phase flow model. This simple approach is further extended to include the compaction of fractured caprocks, the sorption-induced swelling of shale matrix in the fracture-matrix system, the capillary pressure in the two-phase flow system, and fluid property. Based on these preliminary investigations, the following understandings and conclusions can be made.

First, this simple approach can describe the square root law for both pressuring time and pressure magnitude. It can give a fast assessment of caprock sealing efficiency when partial information at the beginning is available. However, the slope of penetration depth versus pressuring time in square root domain depends on the multiphysical interactions among $CO_2$ flow and sorption, rock deformation, as well as the modification of porosity and permeability. Therefore, the slope is a comprehensive parameter for the multiphysical interactions. This simple approach provides a fast assessment method for the $CO_2$ caprock sealing efficiency in natural shale caprocks.

Second, both pressure difference and pressuring time follow a square root law. For incompressible fluid, pressure magnitude in the caprock has no effect on penetration speed. For compressible fluid, both pressure difference and pressure ratio impact the $CO_2$ penetration speed. Therefore, burial depth has some impact on the $CO_2$ penetration depth.

Third, the caprock compaction, the swelling of shale matrix due to $CO_2$ diffusion and the geochemical reaction between fracture and matrix may be the mechanisms for self-enhancement or self-limiting in the $CO_2$-brine mixing zone and the $CO_2$ sweeping zone. These factors may alter the penetration path in the square root spaces of pressure or time.

Finally, the combination of anisotropic swelling and dehydration in the saturated shale caprock may reopen the fracture system, thus enhancing the caprock permeability and reducing the caprock sealing efficiency. This is a potential risk for the $CO_2$ storage in the geological formation and should be further investigated.

## Conflict of interest

The authors wish to confirm that there are no known conflicts of interest associated with this publication and there has been no significant financial support for this work that could have influenced its outcome.

## Acknowledgments

## References

Abidoye LK, Khudaida KJ, Das DB. Geological carbon sequestration in the context of two-phase flow in porous media: a review. Critical Reviews in Environmental Science and Technology 2015;45(11):1105–47.

Anchliya A, Ehlig-Economides C, Jafarpour B. Aquifer management to accelerate $CO_2$ dissolution and tapping. SPE Journal 2012;17(3):805–16.

Andersen O, Gasda SE, Nilsen HM. Vertically averaged equations with variable density for $CO_2$ flow in porous media. Transport in Porous Media 2015;107(1):95–127.

Armitage PJ, Faulkner DR, Worden RH. Caprock corrosion. Nature Geoscience 2013;6:79–80.

Armitage PJ, Worden RH, Faulkner AC, Butcher AR, Espie AA. Permeability of the Mercia mudstone: suitability as caprock to carbon capture and storage sites. Geofluids 2015. http://dx.doi.org/10.1111/gfl.12134.

Barton N. Shear strength criteria for rock, rock joints, rockfill and rock masses: problems and some solutions. Journal of Rock Mechanics and Geotechnical Engineering 2013;5(4):249–61.

Bielicki JM, Peters CA, Fitts JP, Wilson EJ. An examination of geologic carbon sequestration policies in the context of leakage potential. International Journal of Greenhouse Gas Control 2015;37:61–75.

Birkholzer JT, Zhou Q, Tsang CF. Large-scale impact of $CO_2$ storage in deep saline aquifers: a sensitivity study on pressure response in stratified systems. International Journal of Greenhouse Gas Control 2009;3(2):181–94.

Boait FC, White NJ, Bickle MJ, Chadwick RA, Neufeld JA, Huppert HE. Spatial and temporal evolution of injected $CO_2$ at the Sleipner Field, North Sea. Journal of Geophysical Research: Solid Earth 2012;117(B3). http://dx.doi.org/10.1029/2011JB008603.

Bolourinejad P, Herber R. Experimental and modeling study of salt precipitation during injection of $CO_2$ contaminated with $H_2S$ into depleted gas fields in the Northeast of the Netherlands. SPE Journal 2014;19(6):1058–68.

Bricker SH, Barkwith A, MacDonald AM, Hughes AG, Smith M. Effects of $CO_2$ injection on shallow groundwater resources: a hypothetical case study in the Sherwood Sandstone aquifer, UK. International Journal of Greenhouse Gas Control 2012;11:337–48.

Briggs S, Karney BW, Sleep BE. Numerical modelling of flow and transport in rough fractures. Journal of Rock Mechanics and Geotechnical Engineering 2014;6(6):535–45.

Court B, Bandilla KW, Celia MA, Janzen A, Dobossy M, Nordbotten JM. Applicability of vertical-equilibrium and sharp-interface assumptions in $CO_2$ sequestration modeling. International Journal of Greenhouse Gas Control 2012;10:134–47.

Crank J. The mathematics of diffusion. 2nd ed. Oxford, UK: Oxford University Press; 1975.

Dalkhaa C, Shevalier M, Nightingale M, Mayer B. 2-D reactive transport modeling of the fate of $CO_2$ injected into a saline aquifer in the Wabamun Lake Area, Alberta, Canada. Applied Geochemistry 2013;38:10–23.

Deng H, Ellis BR, Peters CA, Fitts JP, Crandall D, Bromhal GS. Modifications of carbonate fracture hydrodynamic properties by $CO_2$ acidified brine flow. Energy & Fuels 2013;27:4221–31.

Deng H, Fitts JP, Crandall D, McIntyre D, Peter CA. Alterations of fractures in carbonate rocks by $CO_2$-acidified brines. Environmental Science and Technology 2015;49(16):10226–34.

Doughty C. Investigation of $CO_2$ plume behavior for a large-scale pilot test of geologic carbon storage in a saline formation. Transport in Porous Media 2010;82:49–76.

Elkhoury JE, Detwiler RL, Ameli P. Can a fractured caprock self-heal? Earth and Planetary Science Letters 2015;417:99–106.

Ellis BR, Fitts JP, Bromhal GS, McIntyre DL, Tappero R, Peters CA. Dissolution-driven permeability reduction of a fractured carbonate caprock. Environmental Engineering Science 2013;30(4):187–93.

Fan Y, Durlofsky LJ, Tchelepi HA. A fully-coupled flow-reactive-transport formulation based on element conservation, with application to $CO_2$ storage simulations. Advances in Water Resources 2012;42:47–61.

Farokhpoor R, Bjorkvikb BJA, Lindeberg E, Torsaeter O. Wettability behaviour of $CO_2$ at storage conditions. International Journal of Greenhouse Gas Control 2013;12: 18–25.

Fei WB, Li Q, Wei XC, Song RR, Jing M, Li XC. Interaction analysis for $CO_2$ geological storage and underground coal mining in Ordos Basin, China. Engineering Geology 2015;196:194–209.

Fontenot BE, Hunt LR, Hildenbrand ZL, Carlton Jr DD, Oka H, Walton JL, Hopkins D, Osorio A, Bjorndal B, Hu QH, Schug KA. An evaluation of water quality in private drinking water wells near natural gas extraction sites in the Barnett shale formation. Environmental Science & Technology 2013;47(17):10032–40.

Gherardi F, Xu T, Pruess K. Numerical modelling of self-limiting and self-enhancing caprock alteration induced by $CO_2$ storage in a depleted gas reservoir. Chemical Geology 2007;244:103–29.

Golding MJ, Neufeld JA, Hesse MA, Huppert HE. Two-phase gravity currents in porous media. Journal of Fluid Mechanics 2011;678:248–70.

Goodarzi S, Settari A, Zoback MD, Keith DW. Optimization of a $CO_2$ storage project based on thermal, geomechanical and induced fracturing effects. Journal of Petroleum Science and Engineering 2015;134:49–59.

Green C, Ennis-King J. Residual trapping beneath impermeable barriers during buoyant migration of $CO_2$. Transport in Porous Media 2013;98(3):505–24.

Heath JE, Dewers TA, McPherson BJOL, Nemer MB, Kotula PG. Pore-lining phases and capillary breakthrough pressure of mudstone caprocks: sealing efficiency of geologic $CO_2$ storage sites. International Journal of Greenhouse Gas Control 2012;11:204–20.

Hesse MA, Woods AW. Buoyant dispersal of $CO_2$ during geological storage. Geophysical Research Letters 2010;37(1). http://dx.doi.org/10.1029/2009GL041128.

Hou Z, Rockhold ML, Murray CJ. Evaluating the impact of caprock and reservoir properties on potential risk of $CO_2$ leakage after injection. Environmental Earth Science 2012;66(8):2403–15.

Huang X, Bandilla KW, Celia MA, Bachu S. Basin-scale modeling of $CO_2$ storage using models of varying complexity. International Journal of Greenhouse Gas Control 2014;20:73–86.

Huerta NJ, Hesse MA, Bryant SL, Strazisar BR, Lopano CL. Experimental evidence for self-limiting reactive flow through a fractured cement core: implications for time-dependent wellbore leakage. Environmental Science and Technology 2013;47:269–75.

Intergovernmental Panel on Climate Change (IPCC). IPCC special report on carbon dioxide capture and storage. In: Metz B, Davidson O, de Coninck HC, Loos M, Meyer LA, editors. Prepared by working group III of the intergovernmental panel on climate change. Cambridge, UK/New York. NY, USA: Cambridge University Press; 2005.

Jiang P, Li X, Xu R, Wang Y, Chen M, Wang H, Ruan B. Thermal modeling of $CO_2$ in the injection well and reservoir at the Ordos CCS demonstration project, China. International Journal of Greenhouse Gas Control 2014;23:135–46.

Kang Q, Chen L, Valocchi AJ, Viswanathan HS. Pore-scale study of dissolution-induced changes in permeability and porosity of porous media. Journal of Hydrology 2014;517:1049–55.

Li Q, Liu Q, Liu X, Li XC. Application of a health, safety, and environmental screening and ranking framework to the Shenhua CCS project. International Journal of Greenhouse Gas Control 2013;17:504–14.

Li X, Akbarabadi M, Karpyn ZT, Piri M, Bazilevskayae E. Experimental investigation of carbon dioxide trapping due to capillary retention in saline aquifers. Geofluids 2015. http://dx.doi.org/10.1111/gfl.12127.

Li X, Elsworth D. Geomechanics of $CO_2$ enhanced shale gas recovery. Journal of Natural Gas Science and Engineering 2014. http://dx.doi.org/10.1016/J.Jngse.2014.08.010.

Ma J. Review of permeability evolution model for fractured porous media. Journal of Rock Mechanics and Geotechnical Engineering 2015;7(3):351–7.

Macminn CW, Szulczewski ML, Juanes R. $CO_2$ migration in saline aquifers. Part 2. Capillary and solubility trapping. Journal of Fluid Mechanics 2011;668: 321–51.

Martinez MJ, Newell P, Bishop JE, Turner DZ. Coupled multiphase flow and geomechanics model for analysis of joint reactivation during $CO_2$ sequestration operations. International Journal of Greenhouse Gas Control 2013;17:148–60.

Matteo EN, Scherer GW. Experimental study of the diffusion-controlled acid degradation of Class H Portland cement. International Journal of Greenhouse Gas Control 2012;7:181–91.

Matter JM, Kelemen PB. Permanent storage of carbon dioxide in geological reservoirs by mineral carbonation. Nature Geoscience 2009;2:837–41.

Murata J, Ogihara Y, Koshikawa S, Itoh Y. Study on watertightness of concrete. ACI Materials Journal 2004;101(2):107–16.

Noiriel C, Gouze P, Bernard D. Investigation of porosity and permeability effects from microstructure changes during limestone dissolution. Geophysical Research Letters 2004;31(24). http://dx.doi.org/10.1029/2004GL021572.

Orlic B, Wassing BBT. A study of stress change and fault slip in producing gas reservoirs overlain by elastic and viscoelastic caprocks. Rock mechanics and Rock Engineering 2013;46:421–35.

Palmer I, Mansoori J. How permeability depends on stress and pore pressure in coalbeds: a new model. SPE Reservoir Evaluation Engineering 1998;1(6): 539–44.

Peng DY, Robinson DB. A new two-constant equation of state. Industrial and Engineering Chemistry: Fundamentals 1976;15(1):59–64.

Rutqvist J, Tsang CF. A study of caprock hydromechanical changes with $CO_2$ injection into a brine formation. Environmental Geology 2002;42(2):296–305.

Rutqvist J, Vasco DW, Myer L. Coupled reservoir-geomechanical analysis of $CO_2$ injection and ground deformations at In Salah, Algeria. International Journal of Greenhouse Gas Control 2010;4(2):225–30.

Rutqvist J. Fractured rock stress-permeability relationships from in situ data and effects of temperature and chemical-mechanical couplings. Geofluids 2015;15(1–2):48–66.

Saaltink M, Vilarrasa V, de Gaspari F, Silva O, Carrera J, Rötting TS. A method for incorporating equilibrium chemicals reactions into multiphase flow models for $CO_2$ storage. Advances in Water Resources 2013;62:431–41.

Sadhukhan S, Gouze P, Dutta T. Porosity and permeability changes in sedimentary rocks induced by injection of reactive fluid: a simulation model. Journal of Hydrology 2012;450–451:134–9.

Smith MM, Sholokhova Y, Hao Y, Carroll SA. Evaporite caprock integrity: an experimental study of reactive mineralogy and pore-scale heterogeneity during brine-$CO_2$ exposure. Environmental Science and Technology 2013;47(1):262–8.

Song ZY, Song H, Cao Y, Killough J, Leung J, Huang G, Gao S. Numerical research on $CO_2$ storage efficiency in saline aquifer with low-velocity non-Darcy flow. Journal of Natural Gas Science and Engineering 2015;23:338–45.

Talebian M, Al-Khoury R, Sluys LJ. A computational model for coupled multiphysics processes of $CO_2$ sequestration in fractured porous media. Advances in Water Resources 2013;59:238–55.

Tsang CF, Birkholzer J, Rutqvist J. A comparative review of hydrologic issues involved in geologic storage of $CO_2$ and injection disposal of liquid waste. Environmental Geology 2008;54:1723–37.

Vilarrasa V, Bolster D, Dentz M, Olivella S, Carrera J. Effects of $CO_2$ compressibility on $CO_2$ storage in deep saline aquifers. Transport in Porous Media 2010;85(2):619–39.

Vilarrasa V, Carrera J. Geologic carbon storage is unlikely to trigger large earthquakes and reactivate faults through which $CO_2$ could leak. Proceedings of the National Academy of Sciences of the United States of America 2015;112(19): 5938–43.

Vilarrasa V, Olivella S, Carrera J, Rutqvist J. Long term impacts of cold $CO_2$ injection on the caprock integrity. International Journal of Greenhouse Gas Control 2014;24:1–13.

Vilarrasa V, Silva O, Carrera J, Olivella S. Liquid $CO_2$ injection for geological storage in deep saline aquifers. International Journal of Greenhouse Gas Control 2013;14:84–96.

Wang JG, Ju Y, Gao F, Peng Y, Gao Y. Effect of $CO_2$ anisotropic sorption and swelling on caprock sealing efficiency. Journal of Cleaner Production 2015;103:685–95.

Wang JG, Liu JS, Kabir A. Combined effects of directional compaction, non-Darcy flow and anisotropic swelling on coal seam gas extraction. International Journal of Coal Geology 2013;109–110:1–14.

Wang JG, Peng Y. Numerical modeling for the combined effects of two-phase flow, deformation, gas diffusion and $CO_2$ sorption on caprock sealing efficiency. Journal of Geochemical Exploration 2014;144:154–67.

Wang S, Vafai K, Mukhopadhyay S. Two-phase $CO_2$ migration in tilted aquifers in the presence of groundwater flow. International Journal of Heat and Mass Transfer 2014;77:717–29.

Watts NL. Theoretical aspects of cap-rock and fault seals for single- and two-phase hydrocarbon columns. Marine and Petroleum Geology 1987;4:274–307.

Wriedt J, Deo M, Han WS, Lepinski J. A methodology for quantifying risk and likelihood of failure for carbon dioxide injection into deep saline reservoirs. International Journal of Greenhouse Gas Control 2014;20:196–211.

Yang H, Flower RJ, Thompson JR. Shale-gas plans threaten China's water resources. Science 2013;340:1288.

Yoo JH, Lee HS, Ismail MA. An analytical study on the water penetration and diffusion into concrete under water pressure. Construction and Building Materials 2011;25(1):99–108.

Zhang CL. Sealing of fractures in claystone. Journal of Rock Mechanics and Geotechnical Engineering 2013;5(3):214–20.

Zhao R, Cheng J, Zhang K. $CO_2$ plume evolution and pressure buildup of large-scale $CO_2$ injection into saline aquifers in Sanzhao Depression, Songliao Basin, China. Transport in Porous Media 2012;95(2):407–24.

Zhou X, Burbey TJ, Westman E. The effect of caprock permeability on shear stress path at the aquifer-caprock interface during fluid injection. International Journal of Rock Mechanics and Mining Sciences 2015;77:1–10.

**J.G. Wang** obtained his bachelor and master degrees in Geotechnical Engineering from Tsinghua University (China) and his PhD in Computational Geomechanics from Nagoya University (Japan). He is a professor of Geotechnical Engineering at China University of Mining and Technology, Xuzhou, China. Before he joined China University of Mining and Technology, he had been working as an associate professor at The University of Western Australia for 5 years and as a research scientist at The National University of Singapore for 13 years. He has published 90 SCI papers in refereed international journals so far. One of his papers was awarded highly cited article award by Thomson Reuters (ISI) in May 2005 and 2007 which implied that his paper was at top 1% within its field. His top three citations are 372, 214 and 107 at 2 November 2015 (based on Web of Science). His current research interests include unconventional natural gas recovery, geological storage of carbon dioxide and geomechanics for mining and petroleum industries.